PERGAMON

Journal of Structural Geology 23 (2001) 895–902

JOURNAL OF STRUCTURAL GEOLOGY

www.elsevier.nl/locate/jstrugeo

Quartz *c*-axes orientation determination using the rotating polarizer microscope

F. Fueten*, J.S. Goodchild

Department of Earth Sciences, Brock University, St. Catharines, Ontario, Canada L2S 3A1

Received 22 January 1999; accepted 23 November 2000

Abstract

A fast and accurate optical method to calculate quartz *c*-axis orientations using the rotating polarizer stage and standard thin sections is presented. *c*-Axis orientations are calculated for each pixel and Achsenverteilungsanalyse (AVA) can easily be constructed to study problems that would normally require a prohibitive amount of tedious work. The computer controlled rotating polarizer stage replaces the polarizer and analyzer of the standard petrographic microscope and allows a thin section to remain fixed while the polarizing filters are rotated by stepper motors. Data are collected by stepping the polarizers through a 180° rotation, capturing a frame at each step and extracting information on the intensity of the pixel and position of the polarizers. The position data are used to calculate the trend or trend + 180° of the quartz *c*-axes, while a simple mathematical relationship between intensity and plunge is derived which allows the plunges of *c*-axes to be calculated.
© 2001 Elsevier Science Ltd. All rights reserved.

1. Introduction

The determination of crystallographic orientations of quartz crystals plays an important role in the microstructural analysis of quartz bearing rocks. A number of techniques based on optical measurements (e.g. Martinez, 1958; Turner and Weiss, 1963; Price 1973; Beyna et al., 1990; Heilbronner and Pauli, 1993) as well as the use of the X-ray texture goniometer (Schmid et al., 1981) and SEM electron channeling methods (e.g. Lloyd and Ferguson, 1986) have been developed to measure complete or partial crystallographic orientations of quartz. Since the technique presented here is an optical method, this discussion will restrict itself to that of other optical methods.

Optical methods do not yield a full description of the orientation of the structure but are restricted to measuring the orientation of the *c*-axis only. While the results are most frequently displayed by plotting *c*-axes orientations on equal-area projections, it can be argued that more information is conveyed when the *c*-axis orientation is coupled with its position. This method, called AVA or Achsenverteilungsanalyse (Sander, 1950) maintains the link between orientation and position by means of a map of color-coded grains in which specific colors correspond to specific *c*-axis orientations.

Optical *c*-axis measurements can be obtained in several ways. Measuring *c*-axes with the universal stage (e.g. Turner and Weiss, 1963) is a time consuming and laborious process which does however allow the operator to keep track of a measured grain's position as well as its *c*-axis. The photometric method (Martinez, 1958; Price, 1973, 1980) yields volume weighted pole figures, but the direct link between position and *c*-axis of a grain is lost. Price (1978) overcame this problem by analyzing small areas.

Beyna et al. (1990) demonstrated that it is possible to determine quartz *c*-axis orientations using a set of images taken from thin sections placed on a flat microscope stage. The advantage of this is that each measurement is made with incident light always through an orthogonal cross section, hence, no tilting of the section is required. Their method measures the *c*-axis orientation for each pixel and does not require the segmentation of the image to define individual quartz grains. Although their method is promising, the equations described by Beyna et al. (1990) to calculate *c*-axis trend and plunge cannot be solved directly. The trend and plunge must be approximated from their respective equations for each pixel in the image.

The technique developed by Heilbronner and Pauli (1993), similar to that of Beyna et al. (1990), calculates *c*-axis orientations for each pixel in captured images. Their method requires the use of polished thin sections, monochrome filters and a lambda plate mounted on the lower

* Corresponding author. Tel.: +1-905-688-5550; fax: +1-905-682-9020.
E-mail address: ffueten@craton.geol.brocku.ca (F. Fueten).

0191-8141/01/$ - see front matter © 2001 Elsevier Science Ltd. All rights reserved.
PII: S0191-8141(00)00161-9

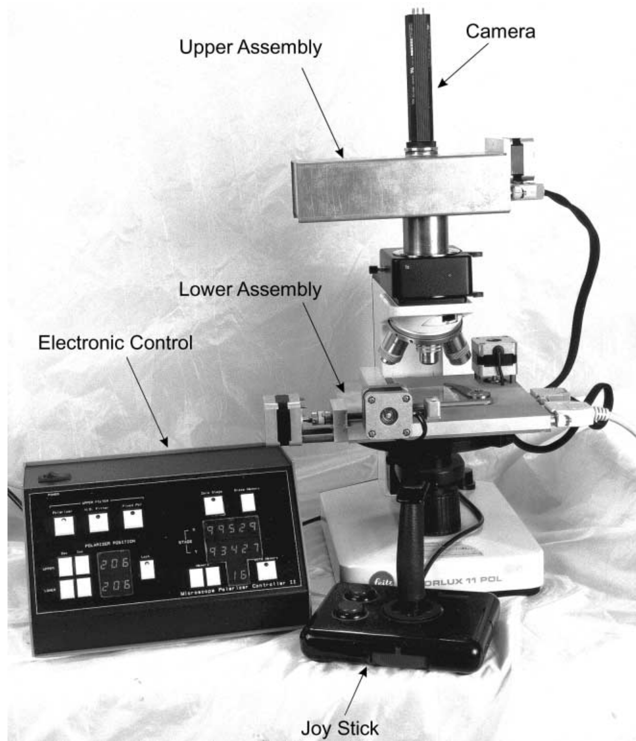

Fig. 1. The Rotating Polarizer Stage. The lower assembly contains the lower rotating polarizer, while the upper rotating polarizer is housed in the upper assembly. The unit also contains an automated *XY* controller not required for the measurements presented here. The design illustrated here allows for more flexibility than the stage originally presented by Fueten (1997).

polarizer. Since the lambda plate produces a color image, and their final data must come in the form of a monochrome intensity, the color information produced by rotating the polarizers is reduced by inserting a monochrome filter into the light path, with the ideal filter determined by the thin section thickness. Heilbronner and Pauli (1993) do not derive analytical equations describing *c*-axes trend and plunge, but instead rely on pre-determined experimental curves when analyzing their data.

Methods that rely on optical measurements from thin sections placed on flat stages alone cannot completely resolve the plunge direction of the *c*-axis. The optical information obtained for a pixel with trend X is the same as for a pixel of trend $X + 180°$. Beyna et al. (1990) do not address this, while Heilbronner and Pauli (1993) overcome this problem by tilting the section and taking a second measurement.

The method presented here is similar in principle to those of Beyna et al. (1990) and Heilbronner and Pauli (1993) in that image processing techniques are applied to captured images and *c*-axes are calculated for each pixel. The technique utilizes the Rotating Polarizer Stage (Fueten, 1997) which has been designed as a general image processing tool for thin sections. The technique is fast, accurate and can be performed on regular thin sections.

2. The rotating polarizer stage

The computer controlled Rotating Polarizer Stage (Fueten, 1997) was designed as a general aid to image processing of petrographic thin sections (Fig. 1). The stage replaces the standard polarizer and analyzer of the petrographic microscope with polarizing filters that are rotated by stepper motors and controlled by a computer which also contains an image capture board. The advantage of using this stage is that the thin section remains fixed while the polarizers are rotated. Hence, any point within a grain is registered to the same pixel at all positions of the polarizers. The standard methodology to collect a sample is to step the polarizers through a 180° rotation under cross-polarized light, followed by a 180° rotation under plane-polarized light. The motors used have a resolution of 0.9° per step, hence a 180° rotation requires 200 steps. At each step, a frame is captured at a resolution of 640×480 pixels in 24-bit color (8 bits each of red, green and blue). A composite data set is constructed that contains selected information obtained for each pixel. The data includes the intensity of the pixels within a grain or the orientation of the polarizing filters at specified intensity values (Fueten, 1997). It takes approximately 2 min to collect a full data set on a 200 MHz PC. The data are used to calculate edges (Goodchild and Fueten, 1998), identify minerals (Goodchild, 1998) as well as to calculate the quartz *c*-axes. Only those aspects of the data set that are relevant for quartz *c*-axes orientations are mentioned here.

2.1. Maximum intensity image

During the sampling process, the intensity (I) of each pixel is calculated in each captured frame using the intensity value (Gonzalez and Woods, 1992) which is defined as

$$I = \frac{(\text{red} + \text{green} + \text{blue})}{3}. \quad (1)$$

The maximum intensity value corresponds to the maximum interference color of a pixel within a grain during a 180° rotation of the polarizers under cross-polarized light. By recording the maximum intensity, intensity variations due to the orientation of the polarizers with respect to the crystal lattice that are evident in single images have been eliminated. Every grain in this image is displayed at its brightest appearance (Fig. 2a). For uniaxial minerals, such as quartz, the maximum intensity is a function of the angle between the *c*-axis and the light path.

2.2. Maximum position image

The position value records the orientation of the polarizing filters, that is the step number, when a pixel reaches its maximum intensity value. Hence, the position value records the orientation of the polarizers with respect to an external reference frame (e.g. that of the microscope or image *XY* axes) when the grain reaches maximum brightness. For a

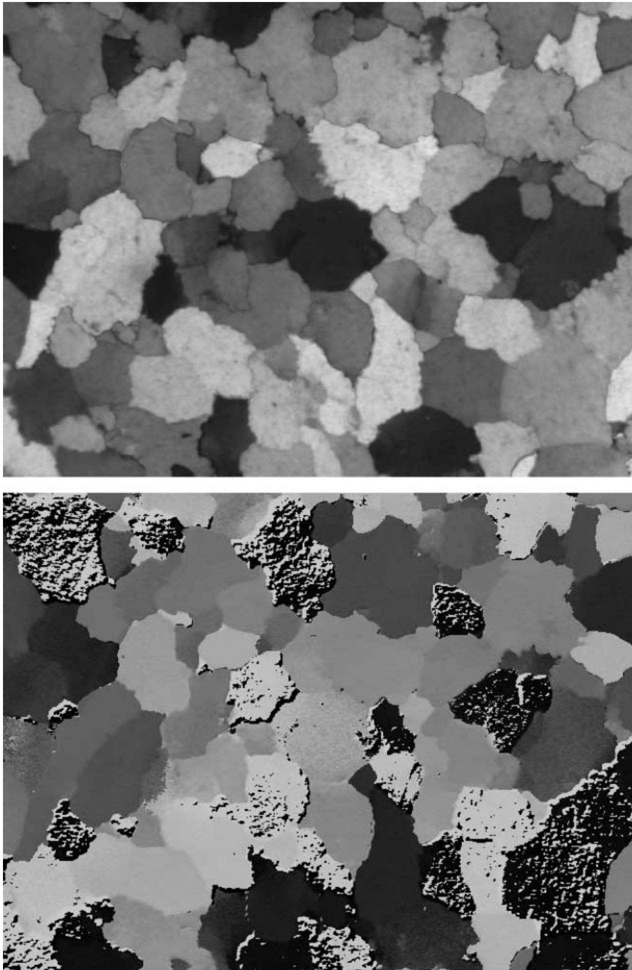

Fig. 2. (a) The maximum intensity image. (Vertical dimension of image is 1.2 mm.) (b) The maximum position image. Grains with a mottled appearance with bright and black pixels have orientations close to 0° and 180°.

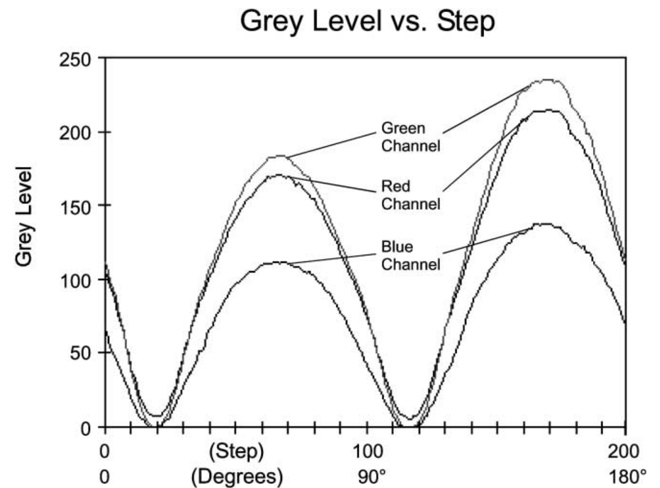

Fig. 3. RGB variations of a single pixel during sampling. The higher peak is recorded for the maximum intensity image. The color differences normally observed by the human eye are too subtle between the two peaks, but are reflected in the differences in their relative RGB percentages.

180° or 200 step rotation, position values have a range of 1–200 and can be represented as gray scale images (Fig. 2b). As will be discussed below, the position value can be directly related to the trend of the quartz *c*-axes.

3. Calculation of trend of the quartz *c*-axes

Standard optical mineralogy (e.g. Nesse, 1986) states that if the vibration directions of a mineral are at 45° to the polarizing direction, the maximum components of the slow and fast rays can be resolved in the analyzer and the mineral appears brightest. Hence, a 180° rotation of a mineral under cross-polarized light conditions will yield two positions of maximum intensity or brightness at 45° and at 135°. In uniaxial minerals, light propagating at an angle to the *c*-axis is split into two vibration directions perpendicular to the wave normal. One vibration direction lies in the (001) plane and is perpendicular to the *c*-axis while the projection of the second vibration direction is parallel to the *c*-axis. Hence, the maximum intensity or brightness for quartz, occurs when the *c*-axis is at angles of 45° and 135° with respect to the lower polarizer vibration direction.

Without the use of accessory plates, the intensity maxima at 45° and at 135° are indistinguishable. Accessory plates increase the retardation between the slow and fast sample rays and enable the differentiation between the two intensity maxima by giving them unique colors. Depending on the thickness of the quartz grain and the type of accessory plate, the maxima at 45° may appear blue, while the maxima at 135° will appear yellow. Heilbronner and Pauli (1993) make use of this phenomenon and add an additional color filter, which nearly completely suppresses one of the maxima.

The technique described here also relies on this phenomenon to calculate the trend of the *c*-axis. As the angle of the vibration directions between the accessory plate and the analyzer must be constant, the accessory plate is permanently mounted below the upper rotating polarizer and rotates with it. Since the rotating polarizer stage is designed as a general image processing tool, an accessory plate which would greatly change the color of the mineral would render the stage useless for mineral identification purposes. Hence, the accessory plate must allow for the distinction of the two peaks but not alter the appearance of the minerals appreciably. After some experimentation it was determined that a sheet of clear anisotropic overhead transparency with a retardation of approximately 115 nm, did sufficiently enhance one maxima (Fig. 3) without altering the appearance of minerals appreciably. The absolute amount of enhancement does vary somewhat with plunge, but is always sufficient to be detected by the camera and video capture board. The color values of the higher peak are recorded in the maximum intensity data, and the position of the polarizers is stored in the maximum position data. Because insertion of the accessory plate can enhance either

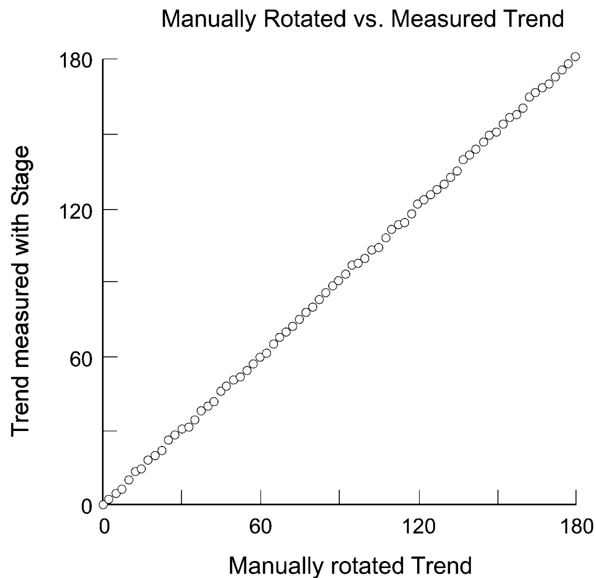

Fig. 4. Trend of a manually rotated quartz grain with horizontal *c*-axis vs trend calculated by rotating polarizer stage. A thin section cut parallel to the *c*-axis of a large single quartz crystal was manually rotated by increments of 2.5° and measured with the computer. This method was chosen to minimize the source of error discussed in the text.

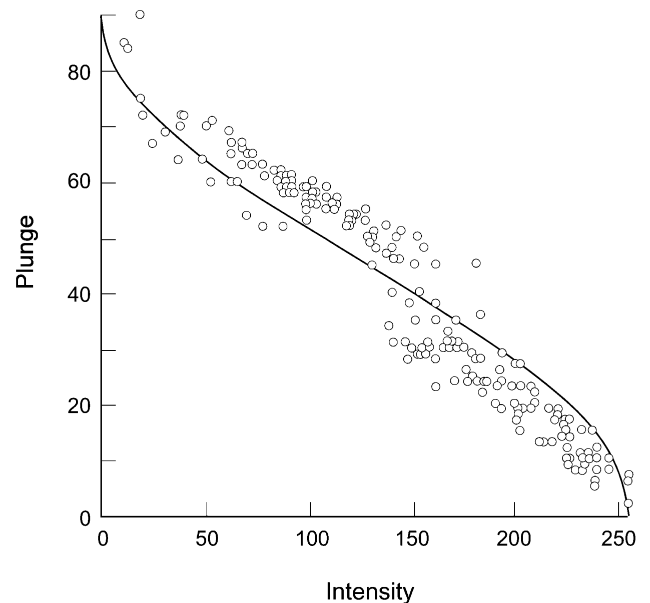

Fig. 5. Plunge vs intensity. The solid line depicts the theoretical relationship (Eq. A8) between plunge and intensity for a maximum intensity of 255. Circles are grains measured manually using a U-stage vs intensity determined by rotating polarizer stage. Part of the step displayed by the actual data is attributed to operator error and part is due to the non-linearity of the camera as discussed in the section on error.

peak, quartz with a known *c*-axis orientation is initially used to determine which peak has been enhanced. In this application the peak at 135° is enhanced; hence, the *c*-axis is at 135° from the polarizer orientation, recorded in the position data. Since we at this stage do not tilt the thin section to take a second reading, the measurement is restricted to yield the trend or the trend + 180°.

The theoretical limit of resolution is given by the step size of 0.9°. To test the actual resolution, a thin section cut parallel to the *c*-axis of a large single quartz crystal was manually rotated by increments of 2.5°. The correspondence between manual rotation and the computer measured *c*-axis orientation (Fig. 4) indicate a maximum discrepancy of 1.6° with an average discrepancy of 0.6°. This illustrates that the actual resolution of the trend of a horizontal *c*-axis is indeed very close to the theoretical limit making the rotating polarizer stage suitable for investigating small changes in *c*-axis orientation such as those observed during subgrain rotation. It is expected that the error is larger for steep *c*-axes.

4. Calculation of plunges of quartz *c*-axes

The magnitude of the maximum intensity reached during a 180° rotation of the polarizers depends on the inclination of the *c*-axis. The greatest intensity is attained when the *c*-axis is horizontal, while the smallest intensity is reached when the *c*-axis is vertical. Unfortunately the relationship between the angle of the *c*-axis and the intensity of the transmitted light is not linear, as is illustrated in Fig. 5. However, a mathematical relationship between the angle of the *c*-axis and the amount of transmitted light can be derived (see Appendix). The relationship is based on the relationship between the angle of the *c*-axis and the ratio of partial birefringence (Eq. (A7)) and the theoretical percentage of light transmission through the analyzer (Price, 1973; Eq. (A8)). The relationship between the *c*-axis plunge angle θ and the maximum intensity I a quartz grain acquires in a 180° rotation is

$$\theta = \frac{1}{2}\cos^{-1}\left[2\frac{I}{I_{max}} - 1\right] \tag{2}$$

where I_{max} is the maximum possible intensity. The intensities I used in Eq. (2) are calculated from the maximum intensity image using Eq. (1) with a range of 0–255.

Arbitrarily assigning I_{max} to a maximum value of 255 assumes that horizontal *c*-axes will always reach an intensity level of 255. However, unless lighting conditions are ideal this will not be the case. Lights that are too bright will generate intensity values of 255 at θ less than 90° while under low illumination 255 will never be reached. Thus, simply assigning the maximum possible intensity to 255 will likely cause errors. In practice I_{max} should be obtained through a calibration process prior to calculating *c*-axes from the measured maximum intensities. This calibration can be performed in several ways.

One method of calibration is to measure the value of I_{max} directly from the thin section being studied. This is accomplished by finding the maximum quartz intensity and assigning that value to I_{max}. The limitation of this method is that it is assumed that the quartz grain producing the highest intensity value has its *c*-axis horizontal. A comparison

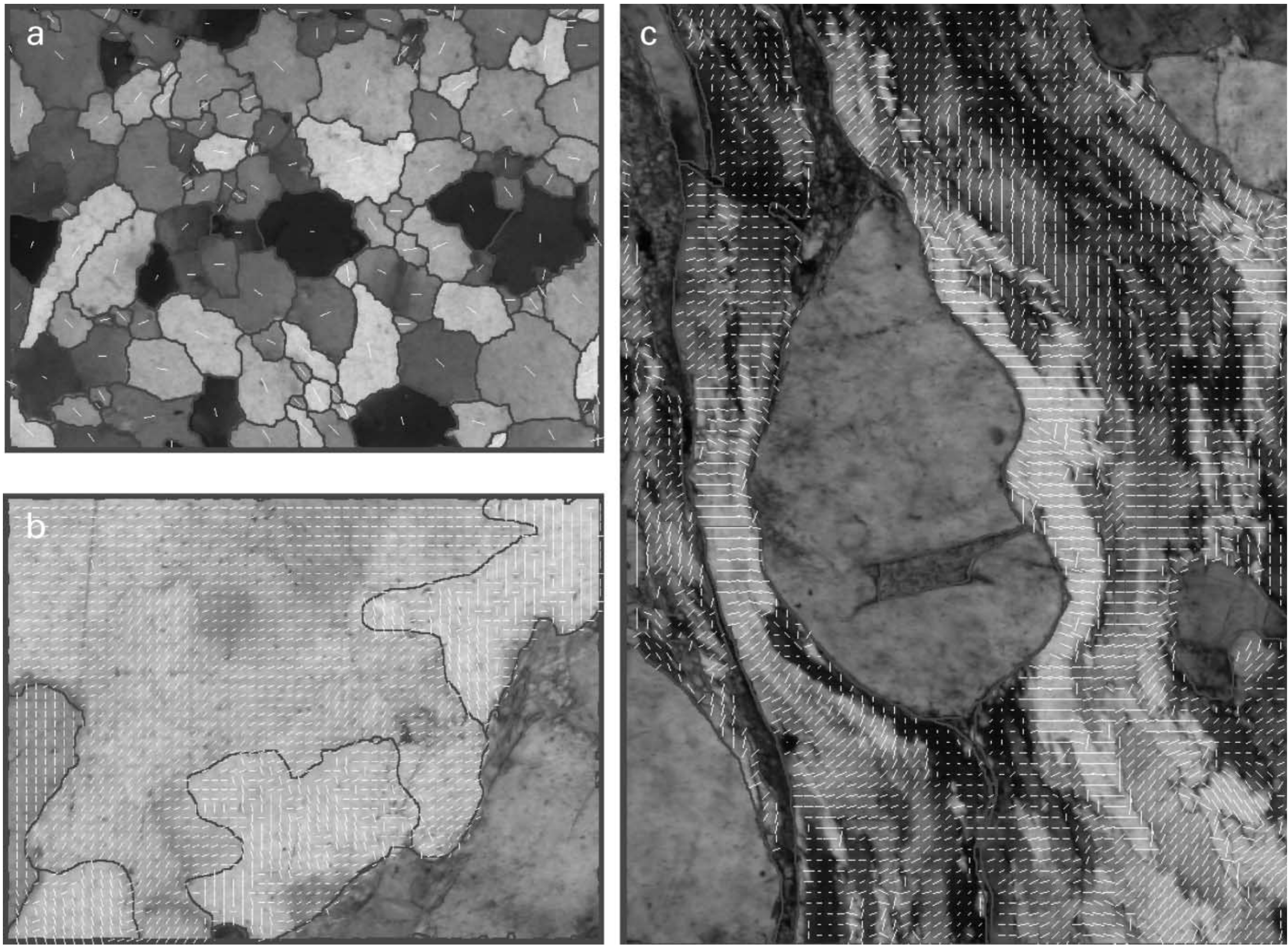

Fig. 6. (a) Maximum intensity image of Fig. 2 with grain boundary and *c*-axes overlay. One *c*-axis is plotted for each grain and scaled according to plunge. Hence, bright grains with shallow axes have long lines while dark grains with steep axes have short lines. (Vertical dimension of image is 1.2 mm.) (b) Maximum intensity image of large quartz grains with subgrains and *c*-axes overlay. *c*-Axis orientations are calculated on a 10×10 grid of pixels. While there is little variation in plunge, as is illustrated by the relatively even illumination, the technique shows the variation of trend well. Axes that are at 90° to their surrounding grid are the result of small inclusions in the quartz, which cause erroneous results. Selecting a larger grid size overcomes this problem. (Vertical dimension of image is 1.2 mm.) (c) Quartz–feldspar mylonite with quartz *c*-axes overlay illustrating the degree of heterogeneity that exists near large clasts. Regions without *c*-axes are feldspar and biotite. Image is a composite view with two individual data sets stitched together. (Vertical dimension of image is 1.2 mm.)

between *c*-axes plunge data measured on the U-stage and theoretically calculated plunge values with I_{max} in Eq. (A8) set to 233 is presented in Fig. 6. The maximum discrepancy between the two data sets is 16° with an average discrepancy of 8.3°, indicating that the plunge calculation is not as accurate as that of the trend. The discrepancy between the two data sets is not random. At low plunges, the calculated plunge based on light intensity is consistently too high while at greater plunges the value based on light intensity is consistently too low. Part of the discrepancy between the data is undoubtedly the result of manual error of measuring the plunge at high angles on the U-stage. However, the consistency of the error is attributed to a non-linear camera response, as is discussed below.

Another, potentially more accurate calibration method requires the measurement of a quartz grain of known orientation (preferably with a horizontal *c*-axis). This would allow for the determination of I_{max} for subsequent samples, assuming there is no change in the lighting condition and the standard and sample thin sections are of equal thickness. Because of these factors, the determination of the plunge is not deemed to be as accurate as the trend.

5. Possible sources of error

The techniques discussed above are susceptible to a number of sources of error which are not normally of concern in a standard microscope and a single frame image capture board. One of the critical requirements for this method is that the intensity of incoming light must remain constant throughout the entire sampling process.

Light fluctuations during the sampling can potentially reduce a major peak or enhance a minor peak, resulting in erroneous measurements. This source of error can be relatively easily controlled with the use of a stabilizing transformer.

Another potential source of error is inherent in the basic design of many microscopes. Not only must the intensity of the incoming light be constant, but that light must also be completely non-polarized. This is not a requirement for microscopes with stationary polarizers, but rotating polarizers above an even weakly polarized light source will result in fluctuations in the amount of polarized light reaching the sample. In many microscopes the light from the bulb is deflected into the light path by means of an inclined mirror, producing weakly polarized light. Similarly, prisms inside some microscope lens assemblies (e.g. macroscopes with a variable zoom) or inside some 3CCD cameras have a weak polarizing effect on the light above the sample, but below the upper polarizing filter. No simple mechanical solution to these problems exists. The easiest solution is to determine the amount of weak polarization that is inherent in the microscope by determining the fluctuations in light levels without a sample and by selecting an accessory plate which induces retardation that exceeds the inherent light fluctuations.

A third potential source of error lies with the electronics of the CCD camera or the video capture board. To obtain data of maximum quality it must be possible to disable any automatic light compensation features (e.g. automatic gain) in the electronics. However, some problems may be inherent in the design of the electronics. For example, the camera used for the data displayed here shows a non-linear response between input light and output RGB values, which cannot be altered. Calibration of the camera indicates that at low light values, it yields higher than expected values, while at higher light intensities it yields lower than expected RGB values. We believe that this non-linearity is largely responsible for the step exhibited in the data in Fig. 5. Adding a correction factor to the code, following a camera calibration, could eliminate this error.

6. Limitations and uses

The procedures outlined above can determine the plunge of the *c*-axes and the trend or trend + 180°. The ambiguity in the trend means that the *c*-axes can, for example, either plunge towards the NW or SE. As stated above, Heilbronner and Pauli (1993) tilt the section and take a second measurement. By comparing the two *c*-axis orientations it is then possible to determine the exact trend and plunge. While it is certainly possible to employ the same solution here, tilting the section for a second measurement is not without its disadvantages. Points in the section that have been registered to the same pixel will inevitably be moved during the second measurement. Depending on the magnification and the field of view, that displacement may be considerable, causing the shifting of grain boundaries. We would argue here that much useful information could in fact be extracted from the data without knowing the true trend obtained in the second measurement. For example, the asymmetries commonly used for shear sense indicators are about the foliation plane of a properly aligned section, and that asymmetry can be obtained by a single measurement.

As argued above, the AVA is one of the most useful ways of displaying *c*-axes data. In a standard AVA, grains are color-coded according to orientation. A color-coded net serves as a legend and the observer is required to make the mental conversion from color to orientation. We much prefer to plot the *c*-axes orientations directly on the image as a line oriented in the direction of the trend (or trend + 180°) and scaled in length according to plunge (Fig. 6). This method of plotting data is similar to the plots of lineations scaled to their plunge that many geologists include on their maps, or to the cells used by Price (1978) and conveys information quickly and intuitively. Data can be plotted for each quartz grain (Fig. 6a), but since *c*-axes are calculated for every pixel, an alternative method is to plot an average *c*-axis at regular grid positions for a chosen grid size. As the procedure is very sensitive to changes in trend, it can be used to examine subgrain orientations within a single grain (Fig. 6b), or produce *c*-axes fields in regions of very fine grained quartz (Fig. 6c) where the plotting of grain boundaries would obscure much data.

One of the practical advantages of the method is its speed. Since the method requires no additional sample preparation and the computational requirements are low, *c*-axes determination, depending on the requirements, can take considerably less than 10 min per sample, with the *c*-axis calculations being essentially instantaneous. On a 200 MHz PC sampling takes <2 min, the edge detection <1.5 min, mineral identification for a quartz-only rock <1 min and *c*-axes calculation <0.5 min.

7. Conclusions

The advantage of the rotating polarizer stage as a tool for structural analysis is that it permits simultaneous examination of features such as grain size, grain shape, grain identity and *c*-axes orientation, allowing for an integrated approach to texture analysis. Because a thin section map or AVA is produced, the orientation data may be spatially correlated with other textural or mineralogical features. Since very small changes in the trend of the *c*-axes can be resolved in this system, the technique may be used for detailed studies, including those involving subgrain rotations. The analysis can be carried out on standard thin sections, which are inexpensive and the most common method of examining microstructures. The method is fast and accurate and while it does not produce the complete crystallographic data provided by TEM or SEM methods, the AVAs

produced by it can easily be used as shear sense indicators or to check for domainal development of *c*-axes. It could certainly be used as a preliminary check before more elaborate methods are employed.

The orientation of quartz *c*-axes can contribute a significant amount of information to many structural studies. It can be argued that the time and effort required gathering the data prevents it from being included in many studies to which it could make a positive contribution. This technique eliminates much of the tedium commonly associated with U-stage analysis and the use of image processing systems has become commonplace. Quartz *c*-axes orientations determined as outlined here could therefore become a standard data set and contribute to many more microstructural studies in quartz bearing rocks.

Information on the manufacture or purchase of a rotating polarizer stage can be obtained by contacting F. Fueten at ffueten@craton.geol.brocku.ca

Acknowledgements

The authors would like to thank the staff of the Technical Services Department at Brock University for their expertise during the construction of the stage. The authors are grateful to J. Starkey for pointing out a problem with an early version of the technique. P. Bons and S. Ralser are thanked for their thorough reviews and insightful suggestions. This work was supported by NSERC Research Grant #OGP0046210.

Appendix. Complete derivation of the equation relating plunge of quartz *c*-axes to maximum intensity under cross-polarized light

The behavior of light as it passes through quartz is modeled by the uniaxial positive indicatrix (Fig. A1). In the uniaxial (positive) indicatrix, the two allowed mutually perpendicular vibration directions will always lie in an elliptical section that is perpendicular to the wave normal direction of the incident light. The vibration directions are parallel to the axes of the elliptical section and the refractive indices define the lengths of the axes.

In Fig. A1(a), the ordinary ray, ω, vibrates parallel to AB and has refractive index n_ω. The component of the extraordinary ray, ε', vibrates parallel to AC and has refractive index n'_ε and the angle between the wave normal (WN) and the optic axis (OA), θ, is equivalent to the angle between n'_ε and the plane of the circular section (Fig. A1b). In any uniaxial mineral, such as quartz, the *c* crystallographic axis is coincident with the optic axis of its indicatrix. It is also known that the wave normal of the incident light on a thin section in a petrographic microscope is vertically oriented. Hence, the angle θ, in Fig. A1(a) and (b), can be thought of as defining the angle between the *c* crystallographic axis in a quartz grain and vertical.

One can define the principal section of the uniaxial positive indicatrix in Fig. A1(b) by the equation of an ellipse in polar form:

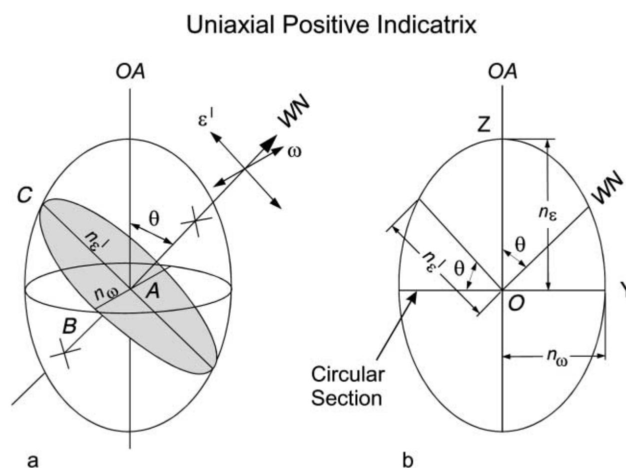

Fig. A1. (a) A uniaxial indicatrix. (b) A principal section through the indicatrix. θ is the angle between the wave normal and the optic axis.

$$\frac{n_\varepsilon'^2 \cos^2\theta}{n_\omega^2} + \frac{n_\varepsilon'^2 \sin^2\theta}{n_\varepsilon^2} = 1, \quad (A1)$$

which can be rearranged to

$$n_\varepsilon'^2 = \frac{n_\omega^2 n_\varepsilon^2}{n_\varepsilon^2 \cos^2\theta + n_\omega^2 \sin^2\theta}. \quad (A2)$$

To solve Eq. (A2) for θ it is desirable to have only one term in the equation that includes θ. Therefore, rearranging Eq. (A2)

$$n_\varepsilon'^2 = \frac{n_\omega^2}{\left(\dfrac{n_\omega^2}{n_\varepsilon^2}\sin^2\theta + \cos^2\theta\right)}. \quad (A3)$$

Substituting $\cos^2\theta = 1 - \sin^2\theta$ in Eq. (A3) and rearranging

$$n_\varepsilon'^2 = \frac{n_\omega^2}{\left(\dfrac{n_\omega^2}{n_\varepsilon^2} - 1\right)\sin^2\theta + 1}. \quad (A4)$$

Eq. (A4) has only one term involving θ, hence it can be solved for θ, which yields

$$\sin^2\theta = \frac{\left(\dfrac{1}{n_\varepsilon'^2} - \dfrac{1}{n_\omega^2}\right)}{\left(\dfrac{1}{n_\varepsilon^2} - \dfrac{1}{n_\omega^2}\right)}. \quad (A5)$$

Using the identity

$$\sin^2\theta = \frac{1}{2} - \frac{1}{2}\cos 2\theta$$

Eq. (A5) becomes

$$\frac{1}{2}-\frac{1}{2}\cos 2\theta=\frac{\left(\frac{1}{n'^2_\varepsilon}-\frac{1}{n^2_\omega}\right)}{\left(\frac{1}{n^2_\varepsilon}-\frac{1}{n^2_\omega}\right)} \quad (A6)$$

which can be rearranged to

$$\theta=\frac{1}{2}\cos^{-1}\left[1-2\frac{\left(\frac{1}{n'^2_\varepsilon}-\frac{1}{n^2_\omega}\right)}{\left(\frac{1}{n^2_\varepsilon}-\frac{1}{n^2_\omega}\right)}\right]. \quad (A7)$$

Eq. (A7) relates the angle between the *c*-axes and vertical to the ratio of partial birefringence to birefringence. However, to utilize this formula one would need to be able to measure n'_ε, n_ε and n_ω, which cannot easily be done. The solution is to replace the ratio of partial birefringence to birefringence with the ratio of maximum intensity attained in a 180° rotation to maximum possible intensity in a 180° rotation. The justification for this is as follows.

The theoretical percentage light transmission through the analyzer given by Price (1973) (see also McKie and McKie, 1974) is

$$I=\cos^2\phi-\sin 2(\tau-\phi)\sin 2\tau\sin^2\left(\frac{\pi d(n'_\varepsilon-n_\omega)}{\lambda}\right) \quad (A8)$$

where I represents the percentage of light transmitted through the analyzer; ϕ represents the angle between the allowed vibration directions in the polarizer and analyzer; τ represents the angle between the polarizer's allowed vibration direction and the quartz grain's closest allowed vibration direction; d represents the thickness of the sample; and λ represents the wavelength of the light.

In this study, all measurements were made at $\phi=90°$ (crossed polars) and at the position of maximum intensity $\tau=135°$. Substituting these values into Eq. (A8) produces

$$I=\sin^2\frac{\pi d(n'_\varepsilon-n_\omega)}{\lambda}. \quad (A9)$$

In uniaxial substances, both of the principal refractive indices are wavelength dependent (McKie and McKie, 1974). This means both the size and shape of the indicatrix can vary with wavelength. In quartz, the dispersion of the extraordinary and ordinary rays is small and they follow a similar path. Consequently, the dispersion of the birefringence is negligible. This causes the size of the quartz indicatrix to vary with wavelength, with the shape remaining constant.

For a sample of constant thickness and light of any wavelength, the maximum intensities that different quartz grains in a thin section acquire, are controlled solely by the birefringence of each individual grain in question. Hence, one can approximate the birefringence in a quartz grain by the maximum intensity that grain acquires in a 180° rotation. The term $(1/n'^2_\varepsilon-1/n^2_\omega)$ in Eq. (A7) is replaced with the maximum intensity the mineral grain acquires in a 180° rotation (I); and the term $(1/n^2_\varepsilon-1/n^2_\omega)$ in Eq. (A7) with the maximum possible intensity a quartz grain can acquire in a 180° rotation (I_{max}). Substituting into Eq. (A7) produces

$$\theta=\frac{1}{2}\cos^{-1}\left[1-2\frac{I}{I_{max}}\right]. \quad (A10)$$

Eq. (A10) relates the *c*-axis orientation measured from the vertical to the intensity ratio the grain acquires in a 180° rotation. To have the *c*-axis orientation measured from the horizontal as is customary, θ is replaced with $\pi/2-\theta$ in equation (10). This produces the final equation relating *c*-axis plunge to the maximum intensity a quartz grain acquires in a 180° rotation:

$$\theta=\frac{1}{2}\cos^{-1}\left[2\frac{I}{I_{max}}-1\right]. \quad (A11)$$

References

Beyna, G., Leymarie, P., Buffet, G., Nault, L., 1990. Principe de l'analyse des fabriques d'axes C du quartz par le traitement d'images numeriques. Comptes Rendus Académie Sciences Paris, Série II 310, 1233–1239.

Fueten, F., 1997. A computer controlled rotating polarizer stage for the petrographic microscope. Computers & Geosciences 23, 203–208.

Gonzalez, R.C., Woods, R.E., 1992. Digital Image Processing. Addison-Wesley, Reading, MA.

Goodchild, J.S., 1998. Geological image processing of petrographic thin section using the rotating polarizer stage. M.Sc. thesis, Brock University.

Goodchild, J.S., Fueten, F., 1998. Edge detection in petrographic images using the rotating polarizer stage. Computers & Geosciences 24, 745–751.

Heilbronner, R.P., Pauli, C., 1993. Integrated spatial and orientation analysis of quartz *c*-axes by computer aided microscopy. Journal of Structural Geology 15, 369–382.

Lloyd, G.E., Ferguson, C.C., 1986. A spherical electron-channelling pattern map for use in quartz petrofabric analysis. Journal of Structural Geology 8, 517–526.

Martinez, J.D., 1958. Photometer method for studying quartz grain orientation. Bulletin of the American Association of Petroleum Geologists 42 (3), 588–608.

McKie, C., McKie, D., 1974. Crystalline Solids. Halsted Press, New York.

Nesse, W.D., 1991. Introduction to Optical Mineralogy. 2nd ed. Oxford University Press, New York.

Price, G.P., 1973. The photometric method in microstructural analysis. American Journal of Sciences 273, 523–537.

Price, G.P., 1978. Study of heterogeneous fabric and texture within a quartz–feldspar mylonite using the photometric method. Bulletin of the Geological Society of America 89, 1359–1372.

Price, G.P., 1980. The analysis of quartz *c*-axis fabrics by the photometric method. Journal of Geology 88, 181–195.

Sander, B., 1950. Einführung in die Gefügekunde der geologischen Körper, zweiter Teil: Die Korngefüge. Springer, Wien.

Schmid, S.M., Casey, M., Starkey, J., 1981. An illustration of the advantages of a complete texture analysis described by the orientation distribution function (ODF) using quartz pole figure data. Tectonophysics 78, 101–117.

Turner, F.J., Weiss, L.E., 1963. Structural Analysis of Metamorphic Tectonites. McGraw-Hill, New York.